

A Binarizing NUV Prior and its Use for M-Level Control and Digital-to-Analog Conversion

Raphael Keusch and Hans-Andrea Loeliger

Abstract—Priors with a NUV representation (normal with unknown variance) have mostly been used for sparsity. In this paper, a novel NUV prior is proposed that effectively binarizes. While such a prior may have many uses, in this paper, we explore its use for discrete-level control (with $M \geq 2$ levels) including, in particular, a practical scheme for digital-to-analog conversion. The resulting computations, for each planning period, amount to iterating forward-backward Gaussian message passing recursions (similar to Kalman smoothing), with a complexity (per iteration) that is linear in the planning horizon. In consequence, the proposed method is not limited to a short planning horizon and can therefore outperform “optimal” methods. A preference for sparse level switches can easily be incorporated.

Index Terms—Discrete-level priors, normals with unknown variance (NUV), finite-control-set model predictive control (MPC), digital-to-analog conversion (DAC).

I. INTRODUCTION

Consider the classical control problem of steering an analog physical linear system along some desired trajectory, or to make the system produce some desired analog output signal. In this paper, we are interested in the special case where the control input is discrete-level (e.g., restricted to M levels), which makes the problem much harder. This discrete-level control problem includes, in particular, a certain type of digital-to-analog converter where the binary (or ternary) output of some digital processor directly drives a continuous-time analog linear filter—preferably an inexpensive one—which produces the desired analog waveform.

It is tempting to ask for an optimal discrete-level control signal, i.e., a control signal that produces the best approximation of the desired analog trajectory (e.g., for a quadratic cost function). However, determining such an optimal control signal is a hard combinatorial optimization problem with a computational complexity that is exponential in the planning horizon [1], [2]. In consequence, insisting on an optimal control signal effectively limits us to a short planning horizon, which is a very severe restriction. This problem is well known in model predictive control (MPC) [3], [4]. Techniques such as sphere decoding do help [5], but the fundamental problem remains.

Clearly, the discrete-level input control problem is a nonconvex optimization problem. A general approach to nonconvex optimization is to resort to some convex relaxation, and to

project the solution back to the permissible set [6]. Another approach uses ideas from sum-of-absolute-values (SOAV) optimization [7], which is an extended version of L_1 optimal control. More general approaches include heuristic methods such as random-restart hill-climbing [8] and simulated annealing [9].

The heart of the method proposed in this paper is a new binarizing NUV prior, where “NUV” stands for “normal with unknown variance”. NUV priors are a central idea of sparse Bayesian learning [10], [11], [12], [13], and closely related to variational representations of L_p -norms [14], [15]. Such priors have been used mainly for sparsity; in particular, no discrete-level-enforcing NUV prior seems to have been proposed in the prior literature. (An interesting non-NUV binarizing prior has been proposed in [16].)

A main advantage of NUV priors in general is their computational compatibility with linear Gaussian models, cf. [17]. In this paper, the computations (for each planning period) amount to iterating forward-backward Gaussian message passing recursions similar to Kalman smoothing, with a complexity (per iteration) that is linear in the planning horizon. In consequence, the proposed method can effectively handle long planning horizons, which can far outweigh its finding only a local minimum of the fitting cost.

The paper is organized as follows. In Section II, we introduce the new NUV prior and demonstrate its binarizing effect in a scalar setting with two pertinent theorems. In Section III, we proceed to the binary-control problem, and the empirical effectiveness of the proposed approach is demonstrated in Sections IV–V-A. In Section VI, we propose and demonstrate a generalization to $M > 2$ levels, and in Section VII, we show how a preference for sparse level switches can be easily be incorporated.

II. THE BINARIZING NUV PRIOR

Let $\mathcal{N}(x; \mu, \sigma^2)$ denote the normal probability density function in x with mean $\mu \in \mathbb{R}$ and variance σ^2 . Let

$$\rho(x, \theta) \triangleq \mathcal{N}(x; a, \sigma_a^2) \mathcal{N}(x; b, \sigma_b^2), \quad (1)$$

where $\theta \triangleq (\sigma_a^2, \sigma_b^2)$ is a shorthand for the two variances in (1). The starting point of this paper is the observation that $\rho(x, \theta)$ can be used as a (improper) joint prior for X and θ that strongly encourages X to lie in $\{a, b\}$.

Before examining this binarizing property, we first note that, for fixed variances θ , $\rho(x, \theta)$ is a Gaussian probability density in x (up to a scale factor). Specifically, $\rho(x, \theta)$ can be written as

$$\rho(x, \theta) = p(x|\theta)p(\theta) \quad (2)$$

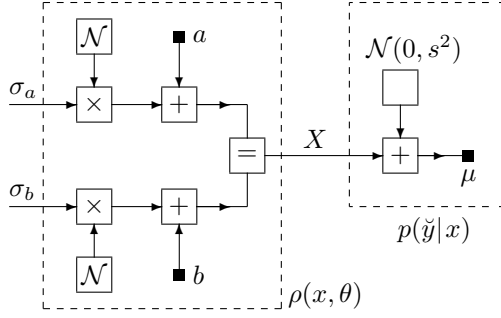


Fig. 1. Factor graph of (8) for fixed \tilde{y} , with parameters μ and s^2 depending on \tilde{y} . The boxes labeled “ \mathcal{N} ” represent normal probability density functions $\mathcal{N}(0, 1)$.

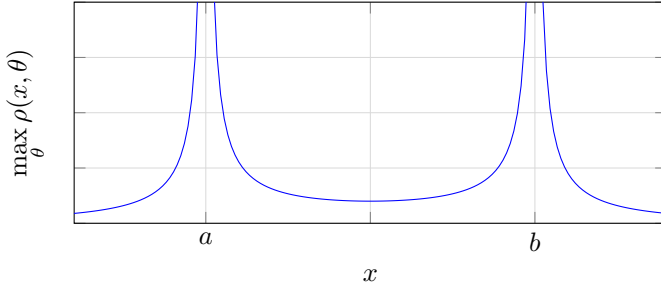


Fig. 2. The effective (improper) prior (12) clearly favors a and b .

with

$$p(x|\theta) = \mathcal{N}(x; \mu_\theta, \sigma_\theta^2) \quad (3)$$

and

$$\rho(\theta) = \frac{1}{\sqrt{2\pi(\sigma_a^2 + \sigma_b^2)}} \exp\left(\frac{-(a-b)^2}{2(\sigma_a^2 + \sigma_b^2)}\right), \quad (4)$$

where

$$\mu_\theta \triangleq \frac{b\sigma_a^2 + a\sigma_b^2}{\sigma_a^2 + \sigma_b^2} \quad (5)$$

and

$$\sigma_\theta^2 \triangleq (1/\sigma_a^2 + 1/\sigma_b^2)^{-1} = \frac{\sigma_a^2 \sigma_b^2}{\sigma_a^2 + \sigma_b^2} \quad (6)$$

The proof of (2)–(6) is given in Appendix A.

In order to study the binarizing effect of the prior (1), we now assume for the rest of this section that $\rho(x, \theta)$ is used in some model with fixed observation(s) \tilde{y} and likelihood function $p(\tilde{y}|x)$. Moreover, we assume $p(\tilde{y}|x)$ to be Gaussian in x , with mean μ and variance s^2 depending on \tilde{y} , i.e.,

$$p(\tilde{y}|x) = \gamma \mathcal{N}(x; \mu, s^2), \quad (7)$$

where γ is an irrelevant scale factor. A factor graph [18] of the resulting statistical system model

$$p(\tilde{y}|x)\rho(x, \theta) = \gamma \mathcal{N}(x; \mu, s^2) \mathcal{N}(x; a, \sigma_a^2) \mathcal{N}(x; b, \sigma_b^2) \quad (8)$$

is shown in Fig. 1.

The detailed working of the binarizing effect of $\rho(x, \theta)$ depends on how the unknown variances θ are determined. Two different ways to estimate these variances are considered in Sections II-A and II-B.

A. Joint MAP Estimation

An obvious approach to estimate x and θ is by joint MAP estimation, which results in

$$\hat{x} = \operatorname{argmax}_x \max_{\theta} p(\tilde{y}|x) \rho(x, \theta) \quad (9)$$

$$= \operatorname{argmax}_x p(\tilde{y}|x) \max_{\theta} \rho(x, \theta) \quad (10)$$

$$= \operatorname{argmax}_x \frac{\mathcal{N}(x; \mu, s^2)}{|x-a| \cdot |x-b|} \quad (11)$$

where the last step follows from

$$\max_{\theta} \rho(x, \theta) = \max_{\sigma_a^2} \mathcal{N}(x; a, \sigma_a^2) \max_{\sigma_b^2} \mathcal{N}(x; b, \sigma_b^2) \quad (12)$$

$$\propto \frac{1}{|x-a| \cdot |x-b|} \quad (13)$$

where “ \propto ” denotes equality up to a scale factor. It is obvious that the effective prior (13), which is plotted in Fig 2, has a strong preference for x to lie in $\{a, b\}$. The following theorem guarantees that, for sufficiently large s^2 , the maximization in (11) is good-natured and returns $\hat{x} = a$ or $\hat{x} = b$.

Theorem 1. The function

$$x \mapsto \frac{\mathcal{N}(x; \mu, s^2)}{|x-a| \cdot |x-b|} \quad (14)$$

has no local maximum (other than the global maxima at $x = a$ and $x = b$) if and only if

$$s^2 > s_{\text{AM}}^2, \quad (15)$$

where s_{AM}^2 is the only real root of the cubic polynomial (97). \square

The polynomial (97) and the proof are given in Appendix B. Since s_{AM}^2 is the only real root of a cubic polynomial, a closed-form expression for s_{AM}^2 exists, but it is cumbersome. However, s_{AM}^2 is easily computed numerically. The value of s_{AM}^2 as a function of μ is plotted in Fig. 3.

In the scalar setting of this section, the estimate (9) can certainly be computed numerically for any s^2 , but such a brute-force approach does not generalize to the sequence setting of Section III-D. With that generalization in mind, we now consider computing (9) by alternating maximization (AM) over x and θ , which operates by alternating the following two steps for $i = 1, 2, 3, \dots$:

- 1) For fixed $\theta = \theta^{(i-1)} = ((\sigma_a^2)^{(i-1)}, (\sigma_b^2)^{(i-1)})$, compute the MAP estimate

$$\hat{x}^{(i)} = \operatorname{argmax}_x p(\tilde{y}|x) \rho(x, \theta) \quad (16)$$

$$= \left(\frac{1}{\sigma_a^2} + \frac{1}{\sigma_b^2} + \frac{1}{s^2} \right)^{-1} \left(\frac{a}{\sigma_a^2} + \frac{b}{\sigma_b^2} + \frac{\mu}{s^2} \right). \quad (17)$$

- 2) For fixed $x = \hat{x}^{(i)}$, compute

$$\theta^{(i)} = \operatorname{argmax}_{\theta} \rho(x, \theta), \quad (18)$$

which yields

$$(\sigma_a^2)^{(i)} = \operatorname{argmax}_{\sigma_a^2} \mathcal{N}(\hat{x}^{(i)}; a, \sigma_a^2) \quad (19)$$

$$= \left(\hat{x}^{(i)} - a \right)^2 \quad (20)$$

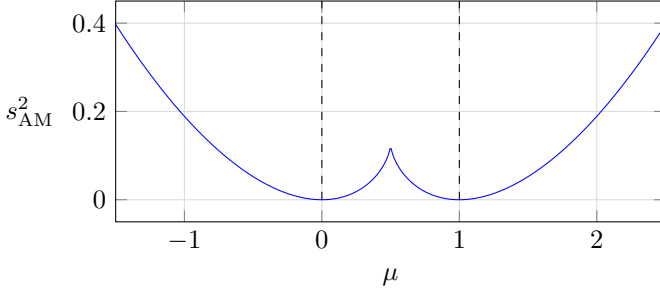


Fig. 3. The value of s_{AM}^2 in (15) as a function of μ for $a = 0$ and $b = 1$.

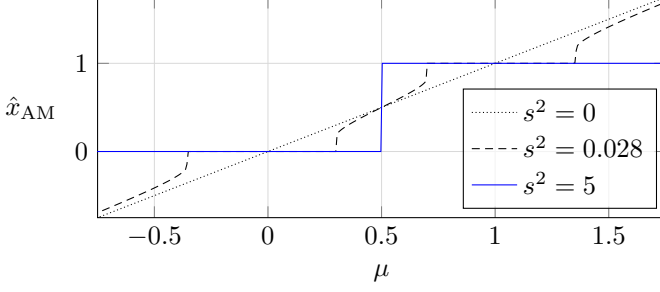


Fig. 4. The estimate of Section II-A for $a = 0$ and $b = 1$, as a function of μ .

and likewise

$$(\sigma_b^2)^{(i)} = (\hat{x}^{(i)} - b)^2. \quad (21)$$

The resulting estimate \hat{x}_{AM} is illustrated in Fig. 4, where σ_a^2 and σ_b^2 were initialized to $(\sigma_a^2)^{(0)} = (\sigma_b^2)^{(0)} = 1$.

For general s^2 , \hat{x}_{AM} need not agree with (9) since AM may converge to a local maximum (or a saddle point). However, if (15) holds, then Theorem 1 guarantees that AM will converge to $\hat{x}_{AM} = a$ or $\hat{x}_{AM} = b$ unless it is unluckily initialized to the (unavoidable) local minimum between a and b .

B. Type-II Estimation¹

Another approach is to first form the MAP estimate

$$\hat{\theta} = \underset{\theta}{\operatorname{argmax}} \int_{-\infty}^{\infty} p(\tilde{y}|x) \rho(x, \theta) \, dx, \quad (22)$$

after which we estimate x as

$$\hat{x} = \underset{x}{\operatorname{argmax}} p(\tilde{y}|x) \rho(x, \hat{\theta}). \quad (23)$$

Note that (23) is given by (17). The difference to the joint-MAP approach of Section II-A is the integration over x in (22). The following theorem guarantees that, for sufficiently large s^2 , the maximization in (22) is good-natured and (23) returns $\hat{x} = a$ or $\hat{x} = b$.

Theorem 2. Assume $a < b$. For $\mu < (a+b)/2$, the function

$$\theta \mapsto \int_{-\infty}^{\infty} \mathcal{N}(x; \mu, s^2) \rho(x, \theta) \, dx \quad (24)$$

¹in the sense of [10], [12]

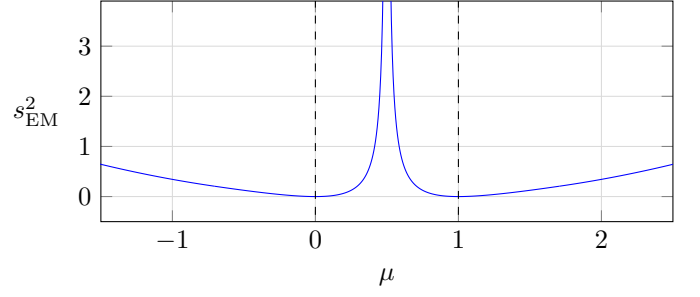


Fig. 5. The value of s_{EM}^2 in (26) and (28) as a function of μ for $a = 0$ and $b = 1$.

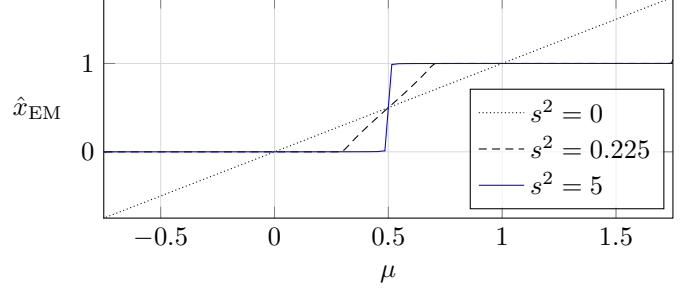


Fig. 6. The estimate of Section II-B for $a = 0$ and $b = 1$, as a function of μ .

has a maximum at $\sigma_a^2 = 0$ and $\sigma_b^2 = (a-b)^2$ (resulting in $\hat{x} = a$) and no other extrema if and only if

$$s^2 > s_{EM}^2, \quad (25)$$

where

$$s_{EM}^2 \triangleq \begin{cases} (3 - \sqrt{8})(a - \mu)(b - \mu), & \text{if } \mu < a - \frac{|a-b|}{\sqrt{2}} \\ \frac{(a-\mu)^2|a-b|}{(a+b)-2\mu}, & \text{if } a - \frac{|a-b|}{\sqrt{2}} \leq \mu < \frac{a+b}{2} \end{cases} \quad (26)$$

Likewise, for $\mu > (a+b)/2$, (24) has a maximum at $\sigma_b^2 = 0$ and $\sigma_a^2 = (a-b)^2$ (resulting in $\hat{x} = b$) and no other extrema if and only if

$$s^2 > s_{EM}^2, \quad (27)$$

where

$$s_{EM}^2 \triangleq \begin{cases} (3 - \sqrt{8})(a - \mu)(b - \mu), & \text{if } \mu > b + \frac{|a-b|}{\sqrt{2}} \\ \frac{(b-\mu)^2|a-b|}{2\mu-(a+b)}, & \text{if } \frac{a+b}{2} < \mu \leq b + \frac{|a-b|}{\sqrt{2}} \end{cases} \quad (28)$$

□

The proof is given in Appendix C. The value of s_{EM}^2 as a function of μ is plotted in Fig. 5.

Having in mind the generalization to the sequence setting (cf. Section III-E), we now consider computing (22) by expectation maximization (EM) [19] with hidden variable X , which operates by computing estimates $\theta^{(1)}, \theta^{(2)}, \dots$ according to

$$\theta^{(i)} = \underset{\theta}{\operatorname{argmax}} \mathbb{E}[\log(p(\tilde{y}|X)\rho(X, \theta))] \quad (29)$$

$$= \underset{\theta}{\operatorname{argmax}} \mathbb{E}[\log \rho(X, \theta)], \quad (30)$$

where the expectation is with respect to $p(x|\tilde{y}, \theta^{(i-1)})$. As will be detailed in Section III-E, the computation of (30) boils down to

$$(\sigma_a^2)^{(i)} = V_X^{(i)} + (\hat{x}^{(i)} - a)^2 \quad (31)$$

TABLE I
STEP 1 OF IKIE IMPLEMENTED BY MBF MESSAGE PASSING WITH INPUT
ESTIMATION ASSEMBLED FROM [17].

The algorithm consists of a forward recursion followed by a backward recursion. The former is a standard Kalman filter, but the latter is not quite standard.

Forward recursion for $k \in \{1, 2, \dots, K\}$, with $\vec{m}_{X_k} \in \mathbb{R}^N$ and $\vec{V}_{X_k} \in \mathbb{R}^{N \times N}$, initialized with the mean \vec{m}_{X_0} and the covariance matrix \vec{V}_{X_0} of X_0 according to $p(x_0)$ in (40).

$$\vec{m}_{X_k} = A(\vec{m}_{X_{k-1}} + \vec{V}_{X_{k-1}} C^T G_{k-1}(\check{y}_{k-1} - C\vec{m}_{X_{k-1}})) + B\vec{m}_{U_k} \quad (\text{M.1})$$

$$\vec{V}_{X_k} = A F_{k-1} \vec{V}_{X_{k-1}} A^T + B \vec{V}_{U_k} B^T \quad (\text{M.2})$$

with

$$G_{k-1} = (s^2 I_L + C \vec{V}_{X_{k-1}} C^T)^{-1} \quad (\text{M.3})$$

$$F_{k-1} = I_N - \vec{V}_{X_{k-1}} C^T G_{k-1} C \quad (\text{M.4})$$

and

$$\vec{m}_{U_k} = \mu_{\theta_k} \text{ as in (5)} \quad (\text{M.5})$$

$$\vec{V}_{U_k} = \sigma_{\theta_k}^2 \text{ as in (6)}. \quad (\text{M.6})$$

Backward recursion for $k \in \{K, K-1, \dots, 1\}$, with $\tilde{\xi}_{X_k} \in \mathbb{R}^N$ and $\tilde{W}_{X_k} \in \mathbb{R}^{N \times N}$, initialized with $\tilde{\xi}_{X_{K+1}} = 0_N$ and $\tilde{W}_{X_{K+1}} = 0_{N \times N}$:

$$\tilde{\xi}_{X_k} = F_k^T A^T \tilde{\xi}_{X_{k+1}} - C^T G_k(\check{y}_k - C\vec{m}_{X_k}) \quad (\text{M.7})$$

$$\tilde{W}_{X_k} = F_k^T A^T \tilde{W}_{X_{k+1}} A F_k + C^T G_k C. \quad (\text{M.8})$$

Output: for $k \in \{1, 2, \dots, K\}$, the posterior mean is

$$\hat{u}_k = \vec{m}_{U_k} - \vec{V}_{U_k} B^T \tilde{\xi}_{X_k} \quad (\text{M.9})$$

and the posterior variance is

$$V_{U_k} = \vec{V}_{U_k} - \vec{V}_{U_k} B^T \tilde{W}_{X_k} B \vec{V}_{U_k}. \quad (\text{M.10})$$

quite stable. For the convenience of readers unfamiliar with the setting of [17], the algorithm is concisely stated in Table I.

D. Determining θ and u by Joint MAP Estimation

Joint MAP estimation of U and θ yields

$$\hat{u} = \arg\max_u \max_{\theta} p(\check{y}|u) \rho(u, \theta). \quad (41)$$

$$= \arg\max_u p(\check{y}|u) \prod_{k=1}^K \max_{\theta_k} \rho_k(u_k, \theta_k). \quad (42)$$

An obvious approach to the maximization over u and θ is to alternate between maximization over u (for fixed θ) and decoupled maximizations over $\theta_1, \dots, \theta_K$ (for fixed u). This procedure is not guaranteed to converge to the global maximum, but it is very practical; in particular, it can be carried out by the IKIE algorithm of Section III-C: Step 1 of IKIE computes the maximizing input signal $\hat{u}^{(i)} = (\hat{u}_1^{(i)}, \dots, \hat{u}_K^{(i)})$ while Step 2 computes the maximizing variances

$$\theta_k^{(i)} = \arg\max_{\theta_k} \rho_k(\hat{u}_k^{(i)}, \theta_k) \quad (43)$$

with

$$(\sigma_{k,a}^2)^{(i)} = \arg\max_{\sigma_{k,a}^2} \mathcal{N}(\hat{u}_k^{(i)}; a, \sigma_{k,a}^2) \quad (44)$$

$$= (\hat{u}_k^{(i)} - a)^2 \quad (45)$$

and likewise

$$(\sigma_{k,b}^2)^{(i)} = (\hat{u}_k^{(i)} - b)^2. \quad (46)$$

E. Determining θ and u by Type-II Estimation Using EM

In this approach, we wish to compute the MAP estimate

$$\hat{\theta} = \arg\max_{\theta} \int_u p(\check{y}|u) \rho(u, \theta) du. \quad (47)$$

A natural approach to this maximization is expectation maximization (EM) [19] with hidden variables U . EM is not guaranteed to compute the global maximum, but it results in a very practical algorithm. Specifically, the update step for θ is

$$\theta^{(i)} = \arg\max_{\theta} \mathbb{E}[\log(p(\check{y}|U) \rho(U, \theta))] \quad (48)$$

$$= \arg\max_{\theta} \mathbb{E}[\log \rho(U, \theta)], \quad (49)$$

where the expectation is with respect to $p(u|\check{y}, \theta^{(i-1)})$. The maximization (49) splits into

$$\theta_k^{(i)} = \arg\max_{\theta_k} \mathbb{E}[\log \rho_k(U_k, \theta_k)], \quad (50)$$

from which we obtain

$$(\sigma_{k,a}^2)^{(i)} = \arg\max_{\sigma_{k,a}^2} \mathbb{E}[\log \mathcal{N}(U_k; a, \sigma_{k,a}^2)] \quad (51)$$

$$= \arg\min_{\sigma_{k,a}^2} \left(\log \sigma_{k,a} + \frac{1}{2\sigma_{k,a}^2} \mathbb{E}[(U_k - a)^2] \right) \quad (52)$$

$$= \mathbb{E}[(U_k - a)^2] \quad (53)$$

and likewise

$$(\sigma_{k,b}^2)^{(i)} = \mathbb{E}[(U_k - b)^2]. \quad (54)$$

The required expectations can be computed by Step 1 of the IKIE algorithm of Section III-C, i.e.,

$$\mathbb{E}[U_k] = \hat{u}_k^{(i)} \quad (55)$$

and

$$\mathbb{E}[U_k^2] = V_{U_k}^{(i)} + \mathbb{E}[U_k]^2, \quad (56)$$

resulting in an IKIE algorithm with Step 2 given by

$$(\sigma_{k,a}^2)^{(i)} = V_{U_k}^{(i)} + (\hat{u}_k^{(i)} - a)^2 \quad (57)$$

and

$$(\sigma_{k,b}^2)^{(i)} = V_{U_k}^{(i)} + (\hat{u}_k^{(i)} - b)^2. \quad (58)$$

F. Remarks

- 1) The parameter s^2 introduced in (39) controls the approximation error (36). If s^2 is chosen too small, the algorithm may return a nonbinary estimate \hat{u} .
- 2) As mentioned, the algorithms of Sections III-D and III-E normally converge to a local (not the global) maximum of (41) and (47), respectively. However, the returned estimate \hat{u} is often very good, cf. Section V-A.
- 3) Both versions of IKIE have the same computational complexity, which is linear in the planning horizon K .

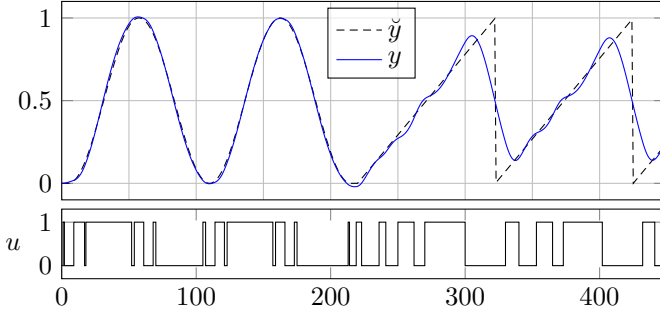


Fig. 8. Digital-to-analog conversion as in Section IV-A with target waveform \check{y} (dashed), digital control signal u (bottom), and filter output signal y (solid blue).

- 4) Empirically, type-II estimation (Section III-E) consistently outperforms joint MAP estimation (Section III-D), which confirms what has long been known for other NUV priors [21]. In the numerical examples in the following sections, only the results with type-II estimation will be reported.
- 5) The generalization of (34) and (35) to time-varying linear systems is obvious and has no effect on the computational cost. Moreover, IKIE is easily adapted to mildly nonlinear systems by adaptive linearization around the momentary trajectory estimate in each iteration.

IV. APPLICATION EXAMPLES

A. Digital-to-Analog Conversion

One method for digital-to-analog conversion is to feed a continuous-time analog linear filter directly with a binary output signal u of a digital processor. This method requires an algorithm to compute a suitable binary signal u such that the analog filter output approximates the desired analog waveform \check{y} . A standard approach is to compute u by a delta-sigma modulator [22], which requires the analog filter to approximate an ideal low-pass filter, which may be costly. By contrast, the method of this paper works also with much simpler (i.e., less expensive) analog filters.

A numerical example with such a converter is shown in Fig. 8. In this example, the analog filter is a simple 3rd-order low-pass, resulting in the discrete-time state space model

$$A = \begin{bmatrix} 0.7967 & -6.3978 & -94.2123 \\ 0.0027 & 0.9902 & -0.1467 \\ 0 & 0.0030 & 0.9999 \end{bmatrix}, \quad (59)$$

$B = [0.0027 \ 0 \ 0]^T$, and $C = [0 \ 0 \ 35037.9]$. The binary input levels are $a = 0$ and $b = 1$. We further have $s^2 = 0.045$ and $K = 450$.

The first half of Fig. 8 shows the normal operation of the digital-to-analog converter, where the target trajectory can be well approximated. The second half of Fig. 8 illustrates what happens if the (unreasonable) target trajectory falls outside the pass band of the analog filter.

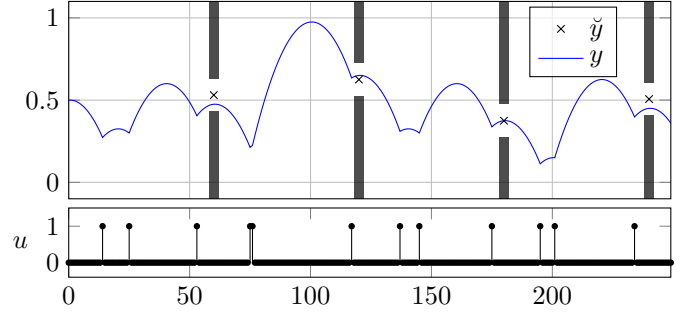


Fig. 9. Flappy bird control with check points \check{y} , binary control signal u (bottom), and resulting trajectory y (solid blue).

B. Trajectory Planning with Sparse Checkpoints

The following control problem is a version of the *flappy bird* computer game [23]. Consider an analog physical system consisting of a point mass m moving forward (left to right in Fig. 9) with constant horizontal velocity and “falling” vertically with constant acceleration g . The $\{0, 1\}$ -valued control signal u affects the system only if $u_k = 1$, in which case a fixed value is added to the vertical momentum. We wish to steer the point mass such that it passes approximately through a sequence of check points, as illustrated in Fig. 9.

For this example, we need a slight generalization⁴ of (34)–(36) as follows. The state $x_k \in \mathbb{R}^2$ (comprising the vertical position and the vertical speed) evolves according to

$$x_k = \begin{bmatrix} 1 & T \\ 0 & 1 \end{bmatrix} x_{k-1} + \begin{bmatrix} 0 \\ 1/m \end{bmatrix} u_k + \begin{bmatrix} 0 \\ -Tg \end{bmatrix}, \quad (60)$$

and we wish the vertical position $y_k = [1 \ 0] x_k$ to minimize

$$\sum_{k=1}^K w_k (y_k - \check{y}_k)^2, \quad (61)$$

where $w_k = 1$ if \check{y}_k is a checkpoint, and $w_k = 0$ otherwise, i.e.,

$$w_k = \begin{cases} 1, & k \in \{60, 120, 180, 240\} \\ 0, & \text{else.} \end{cases} \quad (62)$$

The numerical results in Fig. 9 are obtained with $m = 0.5$, $T = 0.1$, $g = 0.25$, $a = 0$, $b = 1$, $K = 250$, and $s^2 = 0.1$.

V. COMPARISON WITH OTHER METHODS

A. Exhaustive Search

The global minimum of (36) can, in principle, be determined by an exhaustive search. However, the complexity of such a search is exponential in the planning horizon K , which limits its practicability to small K . (Smart versions of tree search such as sphere decoding suffer from the same fundamental limitation.)

By contrast, the algorithms proposed in Section III will normally converge to a local, rather than the global, maximum of (41) or (47). However, in many applications, this deficiency is far outweighed by the ability to easily handle large K .

⁴This generalization is effortlessly handled by IKIE.

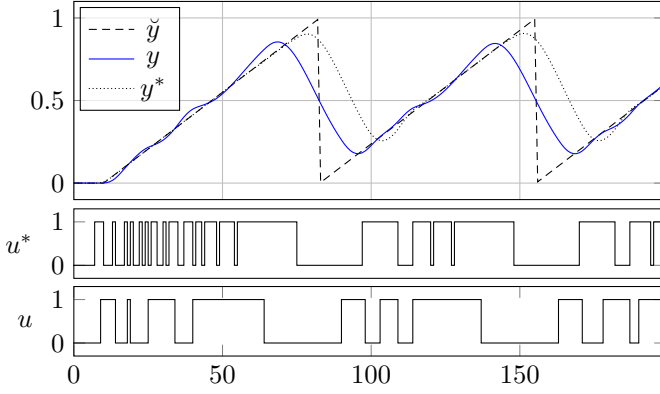


Fig. 10. Comparing the proposed method with an optimal (exhaustive search) controller with planning horizon $K = 8$. The former yields a significantly better approximation (y with $\text{MSE} = 0.01972$) than the latter (y^* with $\text{MSE} = 0.04885$).

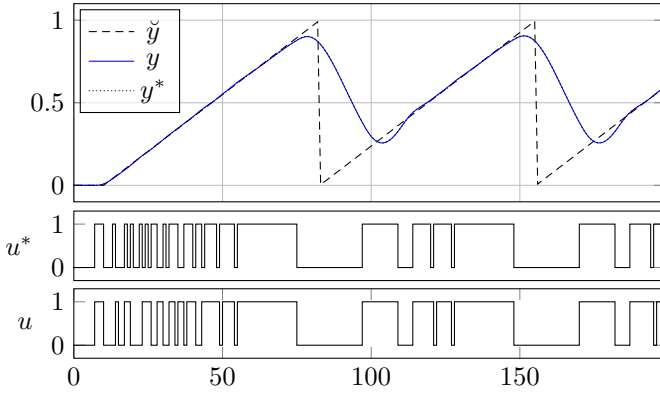


Fig. 11. Comparing the proposed method with planning horizon $K = 8$ with an optimal controller with the same planning horizon. The former yields almost as good a solution (y with $\text{MSE} = 0.04899$) as the latter (y^* with $\text{MSE} = 0.04885$).

For example, Fig. (10) compares an “optimal” (exhaustive search) controller with planning horizon $K = 8$ with the proposed algorithm (IKIE with type-II estimation). The analog system is the same (3rd-order low-pass) as in Section IV-A. The IKIE results are obtained with $s^2 = 0.01$ and full-length K . It is obvious from Fig. 10 that the ability to look sufficiently far ahead is crucial for good performance.

But how suboptimal is the proposed algorithm really? Fig. 11 shows the performance of the proposed algorithm in online mode with the same planning horizon $K = 8$ as the exhaustive-search controller: it turns out, in this example, that the proposed algorithm is very nearly optimal.

B. Other Ways to Gaussify Binary Variables

Non-Gaussian variables can be approximately Gaussified by moment matching (preferably of the posterior), which is the basis of expectation propagation and related methods [24], [25]. While such methods work well in many circumstances, they appear to fail for the examples considered in this paper. (Perhaps such methods have difficulties to choose among different nearly optimal solutions.)

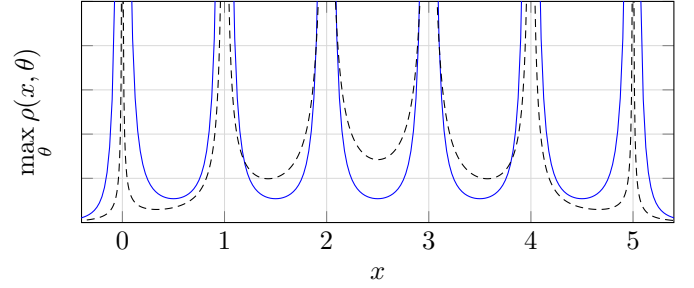


Fig. 12. Generalization of (12) to $M = 6$ equidistant levels. Solid blue: using (66) and (67). Dashed: using (63).

VI. FROM BINARY TO M LEVELS

A. A False Start

An obvious attempt to generalize (1) to more than two levels is

$$\rho(x, \theta) \triangleq \mathcal{N}(x; a, \sigma_a^2) \mathcal{N}(x; b, \sigma_b^2) \mathcal{N}(x; c, \sigma_c^2) \cdots \quad (63)$$

with $\theta \triangleq (\sigma_a^2, \sigma_b^2, \dots)$. However, this turns out not to work very well since it introduces a bias towards the levels in the middle range. The effect is illustrated in Fig. 12, where the dashed line shows the generalization of (12) and Fig. 2 to $\rho(x, \theta)$ as in (63).

B. Adding Binary Variables

Good results are obtained with linear combinations of auxiliary binary (or binarized) variables. For example, constraining X to three levels $\{-b, 0, b\}$ can be achieved by writing

$$X = bX_1 - bX_2 \quad (64)$$

where both X_1 and X_2 are constrained to $\{0, 1\}$ by means of independent priors (1), i.e.,

$$\begin{aligned} \rho(x_1, x_2, \theta_1, \theta_2) &= \mathcal{N}(x_1; 0, \sigma_{1,a}^2) \mathcal{N}(x_1; 1, \sigma_{1,b}^2) \\ &\cdot \mathcal{N}(x_2; 0, \sigma_{2,a}^2) \mathcal{N}(x_2; 1, \sigma_{2,b}^2). \end{aligned} \quad (65)$$

The corresponding generalization of Fig. 6 is shown in Fig. 13.

More generally, we can write X as a linear combination

$$X = \sum_{j=1}^J \beta_j X_j + \beta_0 \quad (66)$$

of independent binary (i.e., binarized to $\{0, 1\}$) variables X_1, \dots, X_J . The choice of J and of the coefficients β_0, \dots, β_J is highly nonunique. Choosing $\beta_j = 2^{j-1}$ for $j > 0$ does not work well empirically. Good results are obtained with

$$\beta_1 = \dots = \beta_J, \quad (67)$$

resulting in $M = J + 1$ equidistant levels for X . (Related representations were used in [26].) The corresponding generalization of (12) is illustrated in Fig. 12. The numerical results in the rest of this paper are all obtained with (67).

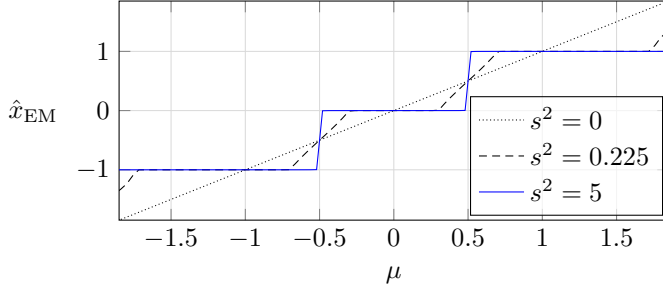


Fig. 13. Generalization of Fig. 6 to three levels $\{-1, 0, 1\}$ using (64).

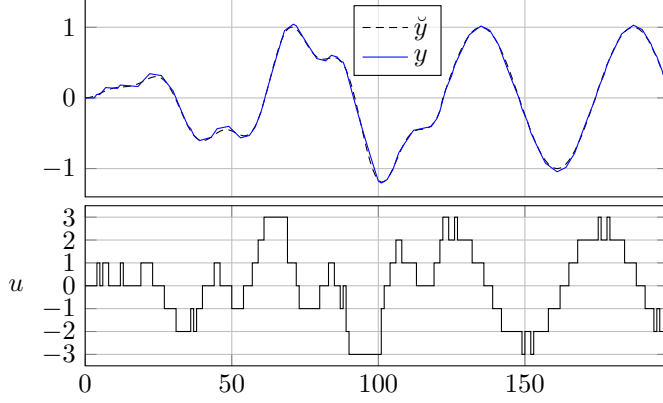


Fig. 14. The example of Section VI-D: M -level control with level set $\{-3, -2, -1, 0, 1, 2, 3\}$, target signal \tilde{y} (dashed), input signal u (bottom), and resulting system output y (blue).

C. Symmetry Breaking

In (66), $X_1 = 0$ and $X_2 = 1$ has the same effect on X as $X_1 = 1$ and $X_2 = 0$. The estimation algorithm must somehow choose among such equivalent configurations. However, depending on the details of the implementation, the estimation algorithm may not, by itself, be able to break such symmetries. This problem can be solved by a slightly asymmetric initialization of the variances, e.g.,

$$\sigma_{1,a}^2 = \sigma_{1,b}^2 \neq \sigma_{2,a}^2 = \sigma_{2,b}^2, \quad (68)$$

where the inequality is almost an equality.

D. Application to M -level Control

Using (66) for the input signal of a state space model as in Section III is straightforward: split the input U_k into independent binarized inputs $U_{k,1}, \dots, U_{k,J}$ according to

$$U_k = \sum_{j=1}^J \beta_j U_{k,j} + \beta_0. \quad (69)$$

The corresponding modification of the state space model is easily handled by the IKIE algorithm.

A numerical example of M -level control with $M = 7$ is shown in Fig. 14, where the system is a simple integrator with parameters

$$A = [0.98], \quad B = [0.05], \quad C = [1], \quad (70)$$

$s^2 = 0.015$ and $K = 200$.

VII. SPARSE LEVEL SWITCHING

In some applications, switching the input signal between the allowed discrete levels is costly (e.g., because of thermal losses in electronic power switches) and should be done as infrequently as possible. Fortunately, the approach of Section III can easily be adapted to address this additional requirement.

A. The Method

The key idea is to extend the state space model such that the level differences $u_k - u_{k-1}$ appear as an additional output signal to which a power penalty can be applied. For binary control, this is achieved by extending (34) and (35) to

$$\tilde{x}_k = \tilde{A}_{k-1} \tilde{x}_{k-1} + \tilde{B} u_k \quad (71)$$

and

$$\tilde{y}_k = \tilde{C} \tilde{x}_k \quad (72)$$

with

$$\tilde{A} = \begin{bmatrix} 0 & 0 & | & 0_{2 \times N} \\ 1 & 0 & | & A \\ \hline 0_{N \times 2} & & & \end{bmatrix}, \quad \tilde{B} = \begin{bmatrix} 1 \\ 0 \\ B \end{bmatrix}, \quad \text{and} \quad (73)$$

$$\tilde{C} = \begin{bmatrix} 1 & -1 & | & 0_{1 \times N} \\ \hline 0_{1 \times N} & & & C \end{bmatrix}, \quad (74)$$

resulting in the extended output signal

$$\tilde{y}_k = \tilde{C} \tilde{x}_k = (u_k - u_{k-1}, y_k). \quad (75)$$

(For M -level control as in Section VI-D, the matrix \tilde{B} is easily modified so that (75) holds also in this case.) We then extend the target signal \tilde{y} to

$$\hat{y} \triangleq (0, \tilde{y}) \quad (76)$$

and the likelihood function (39) to

$$p(\hat{y} | u, \tilde{x}_0) \triangleq \prod_{k=1}^K \frac{1}{(2\pi)^{L/2} \tilde{s}^L} \exp\left(\frac{-\|y_k - \tilde{y}_k\|^2}{2\tilde{s}^2}\right) \cdot \frac{1}{\sqrt{2\pi} \tilde{s}} \exp\left(\frac{-\tilde{y}_{k,1}^2}{2\tilde{s}^2}\right), \quad (77)$$

where $\tilde{y}_{k,1} = u_k - u_{k-1}$ denotes the first component of (76), $\tilde{x}_0 = (0, 0, x_0^T)^T$, and where \tilde{s}^2 is a free parameter which controls the sparsity level of the input signal.

Note that the IKIE algorithm of Section III-C is easily adapted to handle this extended model.

B. An Example

A numerical example with this method is shown in Fig. 15. The system model is an integrator with

$$A = [1], \quad B = [0.1] \quad \text{and} \quad C = [1], \quad (78)$$

which may be viewed as a simple model—an inductor controlled by a voltage input—of an electric motor, where the state variable that we wish to control is the current through the coil.

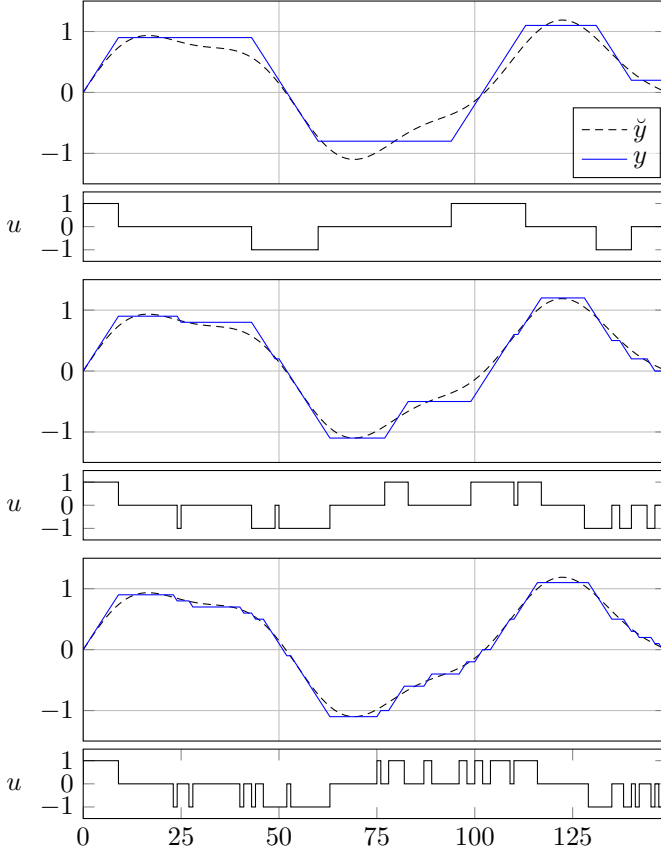


Fig. 15. Motor control as in Section VII-B with target \tilde{y} (dashed), three-level control signal u , and resulting motor coil current y (solid blue). Top: $s^2 = 4$ and $\tilde{s}^2 = 10$; middle: $s^2 = 1$ and $\tilde{s}^2 = 100$; bottom: $s^2 = 0.01$ and $\tilde{s}^2 = 10000$.

VIII. CONCLUSION

We have introduced a new binarizing NUV prior and demonstrated its use for binary and M -level control and digital-to-analog conversion. A preference for sparse level switches can easily be incorporated. The actual computations are iterations of Kalman-type forward-backward recursions, with a complexity (per iteration) that is linear in the planning horizon. This linear complexity compares favorably with existing “optimal” methods. The suitability of the binarizing prior for other applications remains to be investigated.

APPENDIX A PROOF OF (2)–(6)

The claim is that

$$\rho(x, \theta) = \mathcal{N}(x; a, \sigma_a^2) \mathcal{N}(x; b, \sigma_b^2) \quad (79)$$

$$= \frac{1}{\sqrt{2\pi}\sigma_\theta} \exp\left(-\frac{(x - \mu_\theta)^2}{2\sigma_\theta^2}\right) \frac{1}{\sqrt{2\pi(\sigma_a^2 + \sigma_b^2)}} \exp\left(-\frac{(a - b)^2}{2(\sigma_a^2 + \sigma_b^2)}\right). \quad (80)$$

The correctness of the exponents follows from

$$\begin{aligned} & \frac{(x - a)^2}{2\sigma_a^2} + \frac{(x - b)^2}{2\sigma_b^2} - \frac{(x - \mu_\theta)^2}{2\sigma_\theta^2} \\ &= x^2 \left(\frac{1}{2\sigma_a^2} + \frac{1}{2\sigma_b^2} - \frac{1}{2\sigma_\theta^2} \right) - x \left(\frac{a}{\sigma_a^2} + \frac{b}{\sigma_b^2} - \frac{\mu_\theta}{\sigma_\theta^2} \right) \\ & \quad + \frac{a^2}{2\sigma_a^2} + \frac{b^2}{2\sigma_b^2} - \frac{\mu_\theta^2}{2\sigma_\theta^2} \end{aligned} \quad (81)$$

$$= \frac{a^2}{2\sigma_a^2} + \frac{b^2}{2\sigma_b^2} - \frac{(b\sigma_a^2 + a\sigma_b^2)^2}{2(\sigma_a^2 + \sigma_b^2)\sigma_a^2\sigma_b^2} \quad (82)$$

$$= \frac{a^2(\sigma_a^2 + \sigma_b^2)\sigma_b^2 + b^2(\sigma_a^2 + \sigma_b^2)\sigma_a^2 - (b\sigma_a^2 + a\sigma_b^2)^2}{2(\sigma_a^2 + \sigma_b^2)\sigma_a^2\sigma_b^2} \quad (83)$$

$$= \frac{(a^2 - 2ab + b^2)\sigma_a^2\sigma_b^2}{2(\sigma_a^2 + \sigma_b^2)\sigma_a^2\sigma_b^2} \quad (84)$$

$$= \frac{(a - b)^2}{2(\sigma_a^2 + \sigma_b^2)} \quad (85)$$

The correctness of the prefactors follows from

$$\sigma_\theta \sqrt{\sigma_a^2 + \sigma_b^2} = \sigma_a \sigma_b. \quad (86)$$

APPENDIX B PROOF OF THEOREM 1

We examine

$$\mathcal{L}_{\text{AM}}(x) \triangleq -\log \frac{\mathcal{N}(x; \mu, s^2)}{|x - a| \cdot |x - b|} \quad (87)$$

$$\begin{aligned} &= \frac{(\mu - x)^2}{2s^2} + \log |x - a| + \log |x - b| \\ & \quad + \frac{\log(2\pi s^2)}{2}, \end{aligned} \quad (88)$$

which is illustrated in Fig. 16. Clearly, for any $s^2 > 0$, the singularities at $x = a$ and $x = b$ are global minima of (88). Between these two singularities, by continuity, there is at least one local maximum, and there may be additional local minima and maxima.

The derivative of (88) is

$$\frac{\partial}{\partial x} \mathcal{L}_{\text{AM}}(x) = \frac{1}{s^2}(x - \mu) + \frac{1}{x - a} + \frac{1}{x - b} \quad (89)$$

In order to examine the existence of such additional local minima and maxima, we set (89) to zero, which yields

$$c_3 x^3 + c_2 x^2 + c_1 x + c_0 = 0 \quad (90)$$

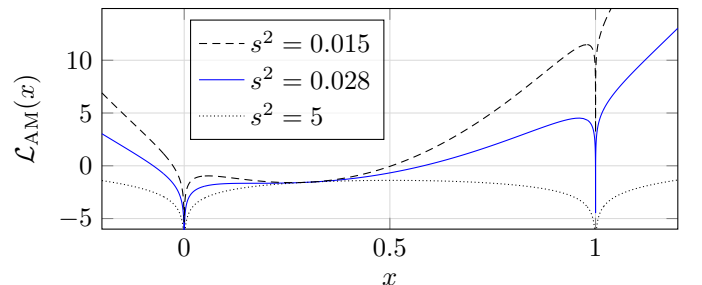


Fig. 16. The cost function (88) for $a = 0$, $b = 1$, $\mu = 0.3$, and different values of s^2 . For small s^2 (dashed), an additional local minimum appears.

with coefficients

$$c_0 = s^2(-a - b) - ab\mu \quad (91)$$

$$c_1 = 2s^2 + ab + (a + b)\mu \quad (92)$$

$$c_2 = -a - b - \mu \quad (93)$$

$$c_3 = 1. \quad (94)$$

The left-hand side of (90) is a cubic polynomial with discriminant

$$\Delta = -27c_3^2c_0^2 + 18c_3c_2c_1c_0 - 4c_3c_1^3 - 4c_2^3c_0 + c_2^2c_1^2. \quad (95)$$

If $\Delta > 0$, then (90) has three real solutions, and if $\Delta < 0$, then (90) has only one real solution. (These two cases are illustrated in Fig. 16 by the dashed line and the dotted line, respectively.) Recall that there is at least one local maximum between a and b . Thus (88) has no local minimum if and only if $\Delta < 0$.

We proceed to examine the condition $\Delta < 0$ as a function of s^2 . The following calculations are very cumbersome and are preferably carried out (or verified) with the aid of computer algebra. We begin by writing (95) as

$$\Delta = \phi(s^2), \quad (96)$$

where ϕ is the polynomial

$$\phi(\zeta) \triangleq \tilde{c}_3\zeta^3 + \tilde{c}_2\zeta^2 + \tilde{c}_1\zeta + \tilde{c}_0 \quad (97)$$

with coefficients

$$\tilde{c}_0 = (a - b)^2(a - \mu)^2(b - \mu)^2 \quad (98)$$

$$\tilde{c}_1 = -2(a - b)^2(2(a^2 + b^2) + ab - 5\mu(a + b - \mu)) \quad (99)$$

$$\tilde{c}_2 = 13(a - b)^2 + 4(ab - a\mu - b\mu + \mu^2) \quad (100)$$

$$\tilde{c}_3 = -32. \quad (101)$$

Since $\tilde{c}_3 < 0$, (96) is negative for sufficiently large s^2 . It remains to show that (97) has exactly one real root. But the discriminant of (97) is

$$\tilde{\Delta} = -27\tilde{c}_3^2\tilde{c}_0^2 + 18\tilde{c}_3\tilde{c}_2\tilde{c}_1\tilde{c}_0 - 4\tilde{c}_3\tilde{c}_1^3 - 4\tilde{c}_2^3\tilde{c}_0 + \tilde{c}_2^2\tilde{c}_1^2 \quad (102)$$

$$= -16(a - b)^2(a + b - 2\mu)^4\gamma^3 \quad (103)$$

with

$$\gamma \triangleq 6(a - b)^2 + a^2 + b^2 + \mu^2 - (ab + a\mu + b\mu). \quad (104)$$

For $a \neq b$, $\gamma > 0$ since $ab < (a^2 + b^2)/2$, $a\mu \leq (a^2 + \mu^2)/2$, and $b\mu \leq (b^2 + \mu^2)/2$. Thus $\tilde{\Delta} < 0$, which implies that (97) has exactly one real root.

APPENDIX C PROOF OF THEOREM 2

A. Rewriting the Function

Using (2) and (3), the function (24) can be written as

$$\begin{aligned} & \int_{-\infty}^{\infty} \mathcal{N}(x; \mu, s^2) \rho(x, \theta) dx \\ &= \rho(\theta) \int_{-\infty}^{\infty} \mathcal{N}(x; \mu, s^2) p(x|\theta) dx \end{aligned} \quad (105)$$

$$= \rho(\theta) \int_{-\infty}^{\infty} \mathcal{N}(\mu; x, s^2) \mathcal{N}(x; \mu_\theta, \sigma_\theta^2) dx \quad (106)$$

$$= \rho(\theta) \mathcal{N}(\mu - \mu_\theta; \sigma_\theta^2 + s^2), \quad (107)$$

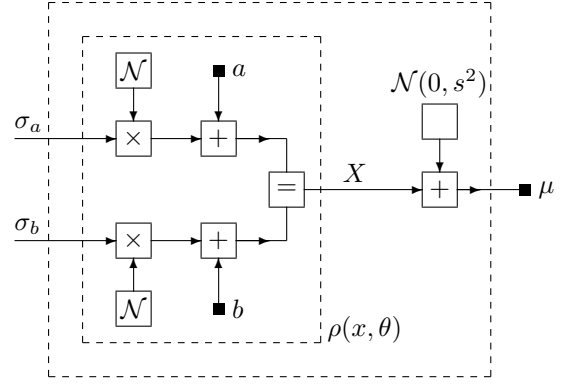


Fig. 17. The step from (106) to (107).

cf. Fig. 17. Inserting (4), taking logarithms, changing the sign, and dropping irrelevant constants yields

$$\begin{aligned} \mathcal{L}_{\text{EM}}(\theta) \triangleq & \log(\sigma_a^2 + \sigma_b^2) + \frac{(a - b)^2}{\sigma_a^2 + \sigma_b^2} \\ & + \log(\sigma_\theta^2 + s^2) + \frac{(\mu - \mu_\theta)^2}{\sigma_\theta^2 + s^2} \end{aligned} \quad (108)$$

Note that the minima and maxima of (108) are exactly the maxima and minima, respectively, of (24).

For $\sigma_a^2 > 0$ and $\sigma_b^2 > 0$, (108) is continuous and differentiable both in σ_a^2 and in σ_b^2 . Moreover, $\lim_{\sigma_a^2 + \sigma_b^2 \rightarrow 0} \mathcal{L}_{\text{EM}}(\theta) = \infty$. In consequence, (108) has at least one minimum for finite $\sigma_a^2 \geq 0$ and $\sigma_b^2 \geq 0$.

In the following, we will occasionally use the assumption $a < b$ from the theorem.

B. Derivatives

$$\begin{aligned} \frac{\partial \mathcal{L}_{\text{EM}}(\theta)}{\partial \sigma_a^2} = & \frac{1}{\sigma_a^2 + \sigma_b^2} - \frac{(a - b)^2}{(\sigma_a^2 + \sigma_b^2)^2} + \frac{1}{\sigma_\theta^2 + s^2} \cdot \frac{\partial \sigma_\theta^2}{\partial \sigma_a^2} \\ & + \frac{2(\mu_\theta - \mu)}{\sigma_\theta^2 + s^2} \cdot \frac{\partial \mu_\theta}{\partial \sigma_a^2} - \frac{(\mu_\theta - \mu)^2}{(\sigma_\theta^2 + s^2)^2} \cdot \frac{\partial \sigma_\theta^2}{\partial \sigma_a^2} \end{aligned} \quad (109)$$

with

$$\frac{\partial \mu_\theta}{\partial \sigma_a^2} = \frac{b}{\sigma_a^2 + \sigma_b^2} - \frac{b\sigma_a^2 + a\sigma_b^2}{(\sigma_a^2 + \sigma_b^2)^2} \quad (110)$$

$$= \frac{(b - a)\sigma_b^2}{(\sigma_a^2 + \sigma_b^2)^2} \quad (111)$$

and

$$\frac{\partial \sigma_\theta^2}{\partial \sigma_a^2} = \left(\frac{\sigma_b^2}{\sigma_a^2 + \sigma_b^2} \right)^2. \quad (112)$$

By symmetry, $\partial \mathcal{L}_{\text{EM}}(\theta) / \partial \sigma_b^2$ is obtained by exchanging a and b , and σ_a^2 and σ_b^2 , in (109)–(112).

C. Binarizing Minima

For $\sigma_b^2 = 0$, (109) becomes

$$\frac{\partial \mathcal{L}_{\text{EM}}(\theta)}{\partial \sigma_a^2} = \frac{\sigma_a^2 - (a - b)^2}{\sigma_a^4} \quad (113)$$

It follows that the point

$$\sigma_b^2 = 0 \quad \text{and} \quad \sigma_a^2 = (a-b)^2 \quad (114)$$

is a minimum of (108) if and only if $\partial \mathcal{L}_{\text{EM}}(\theta)/\partial \sigma_b^2 > 0$. By symmetry, the point

$$\sigma_a^2 = 0 \quad \text{and} \quad \sigma_b^2 = (a-b)^2 \quad (115)$$

is a minimum of (108) if and only if $\partial \mathcal{L}_{\text{EM}}(\theta)/\partial \sigma_a^2 > 0$. We now examine this condition.

At the point (115), we have $\mu_\theta = a$, $\sigma_\theta^2 = 0$, $\partial \sigma_\theta^2/\partial \sigma_a^2 = 1$, and (109) becomes

$$\frac{\partial \mathcal{L}_{\text{EM}}(\theta)}{\partial \sigma_a^2} = \frac{1}{(a-b)^2} - \frac{1}{(a-b)^2} + \frac{1}{s^2} + \frac{2(a-\mu)}{s^2} \cdot \frac{(b-a)}{(a-b)^2} - \frac{(a-\mu)^2}{s^4} \quad (116)$$

$$= \frac{1}{s^2} \left(1 + \frac{2(a-\mu)}{b-a} - \frac{(a-\mu)^2}{s^2} \right) \quad (117)$$

$$= \frac{2}{s^2(b-a)} \left(\frac{a+b}{2} - \mu - \frac{(b-a)(a-\mu)^2}{2s^2} \right) \quad (118)$$

Recalling the assumption $b > a$, it follows that (115) is a minimum of (108) if and only if

$$\mu < \frac{a+b}{2} - \frac{(b-a)(a-\mu)^2}{2s^2} \quad (119)$$

or, equivalently, if and only if $\mu < (a+b)/2$ and

$$s^2 > \frac{(b-a)(a-\mu)^2}{a+b-2\mu} \quad (120)$$

By symmetry, (114) is a minimum of $\mathcal{L}_{\text{EM}}(\theta)$ if and only if

$$\mu > \frac{a+b}{2} + \frac{(b-a)(b-\mu)^2}{2s^2} \quad (121)$$

or, equivalently, if and only if $\mu > (a+b)/2$ and

$$s^2 > \frac{(b-a)(b-\mu)^2}{2\mu - (a+b)} \quad (122)$$

D. Other Extrema — Part I

The rest of the proof is about excluding any other extrema, i.e., extrema with $\sigma_a^2 > 0$ and $\sigma_b^2 > 0$. Such extrema are characterized by the conditions

$$\frac{\partial \mathcal{L}_{\text{EM}}(\theta)}{\partial \sigma_a^2} = 0. \quad (123)$$

and

$$\frac{\partial \mathcal{L}_{\text{EM}}(\theta)}{\partial \sigma_b^2} = 0. \quad (124)$$

The following calculations are very cumbersome and are preferably carried out (or verified) with the aid of computer algebra. We begin by eliminating μ_θ and σ_θ^2 in (109) using (5) and (6), i.e.,

$$\mu_\theta - \mu = \frac{b\sigma_a^2 + a\sigma_b^2 - \mu(\sigma_a^2 + \sigma_b^2)}{\sigma_a^2 + \sigma_b^2} \quad (125)$$

and

$$\sigma_\theta^2 + s^2 = \frac{\sigma_a^2\sigma_b^2 + s^2\sigma_a^2 + s^2\sigma_b^2}{\sigma_a^2 + \sigma_b^2} \quad (126)$$

We thus obtain

$$\begin{aligned} \frac{\partial \mathcal{L}_{\text{EM}}(\theta)}{\partial \sigma_a^2} &= \left(\sigma_a^2\sigma_b^2 + s^2\sigma_a^2 + s^2\sigma_b^2 \right)^{-2} \\ &\cdot \left(\sigma_a^2(s^2 + \sigma_b^2)^2 - \sigma_b^4(a-\mu)^2 - s^4(a-b)^2 \right. \\ &\quad \left. - 2s^2\sigma_b^2(a^2 - a\mu + b\mu - ab) + s^2\sigma_b^2(s^2 + \sigma_b^2) \right). \end{aligned} \quad (127)$$

Note that (127) is a fraction of two polynomials with a strictly positive denominator and a numerator that is linear in σ_a^2 . We can thus solve (123) for σ_a^2 , resulting in

$$\begin{aligned} \sigma_a^2 &= (s^2 + \sigma_b^2)^{-2} \left(\sigma_b^4(a-\mu)^2 + s^4(a-b)^2 \right. \\ &\quad \left. + 2s^2\sigma_b^2(a^2 - a\mu + b\mu - ab) - s^2\sigma_b^2(s^2 + \sigma_b^2) \right). \end{aligned} \quad (128)$$

Likewise, setting (124) to zero yields

$$\begin{aligned} \sigma_b^2 &= (s^2 + \sigma_a^2)^{-2} \left(\sigma_a^4(b-\mu)^2 + s^4(a-b)^2 \right. \\ &\quad \left. + 2s^2\sigma_a^2(b^2 - b\mu + a\mu - ab) - s^2\sigma_a^2(s^2 + \sigma_a^2) \right). \end{aligned} \quad (129)$$

Inserting (129) into (127) yields

$$\left. \frac{\partial \mathcal{L}_{\text{EM}}(\theta)}{\partial \sigma_a^2} \right|_{(124)} = \frac{A_a\sigma_a^4 + B_a\sigma_a^2 + C_a}{(s^2 + \sigma_a^2)^2(s^2(b-a) + \sigma_a^2(b-\mu))} \quad (130)$$

with coefficients

$$A_a = b - \mu \quad (131)$$

$$B_a = s^2(a + 2b - 3\mu) - (a - \mu)^2(b - \mu) \quad (132)$$

$$C_a = s^4(a + b - 2\mu) + s^2(a - \mu)^2(a - b). \quad (133)$$

By symmetry, we likewise obtain

$$\left. \frac{\partial \mathcal{L}_{\text{EM}}(\theta)}{\partial \sigma_b^2} \right|_{(123)} = \frac{A_b\sigma_b^4 + B_b\sigma_b^2 + C_b}{(s^2 + \sigma_b^2)^2(s^2(a-b) + \sigma_b^2(a-\mu))} \quad (134)$$

with coefficients

$$A_b = a - \mu \quad (135)$$

$$B_b = s^2(b + 2a - 3\mu) - (b - \mu)^2(a - \mu) \quad (136)$$

$$C_b = s^4(a + b - 2\mu) + s^2(b - \mu)^2(b - a). \quad (137)$$

The point of these manipulations is that (130) does not depend on σ_b^2 and (134) does not depend on σ_a^2 , and we have

Lemma 1. Eq. (123) and (124) hold simultaneously if and only if (130) and (134) are both zero. \square

E. Other Extrema — Part II

The numerator of (130) is $\phi_a(\sigma_a^2)$ with

$$\phi_a(\zeta) \triangleq A_a\zeta^2 + B_a\zeta + C_a. \quad (138)$$

We thus need to examine the conditions for (138) to have a positive real root. Clearly, (138) has real roots if and only if

$$B_a^2 - 4A_aC_a \geq 0. \quad (139)$$

Plugging in⁵ (131)–(133) turns (139) into

$$(a - \mu)^2\psi(s^2) \geq 0 \quad (140)$$

⁵again preferably done or verified by computer algebra

with

$$\psi(\xi) \triangleq \xi^2 - 6(a - \mu)(b - \mu)\xi + (a - \mu)^2(b - \mu)^2. \quad (141)$$

It is easily verified that $\psi(\xi) = 0$ if and only if

$$\xi = |a - \mu| \cdot |b - \mu| \left(3 \operatorname{sgn}(a - \mu) \operatorname{sgn}(b - \mu) \pm \sqrt{8} \right) \quad (142)$$

where sgn denotes the sign function

$$\operatorname{sgn}(z) \triangleq \begin{cases} +1, & \text{if } z \geq 0 \\ -1, & \text{if } z < 0. \end{cases} \quad (143)$$

If $a < \mu < b$ the zeros of ψ are negative, which implies $\psi(s^2) \geq 0$ for all s^2 . For $\mu \leq a$ or $\mu \geq b$, the zeros of ψ are positive and $\psi(s^2) < 0$ if and only if

$$(3 - \sqrt{8})(a - \mu)(b - \mu) < s^2 < (3 + \sqrt{8})(a - \mu)(b - \mu). \quad (144)$$

By symmetry, the same conditions apply also for the numerator of (134). In summary, we have

Lemma 2. The polynomial (138) has no real zeros—i.e., (139) does not hold—if and only if (144) holds. The same condition applies also to the numerator of (134). \square

We now assume that (139) holds, and we examine the conditions for (138) to have at least one positive root. If $A_a > 0$, then the condition is $-B_a + \sqrt{B_a^2 - 4A_aC_a} \geq 0$; if $A_a < 0$, then the condition is $-B_a - \sqrt{B_a^2 - 4A_aC_a} \leq 0$. These two conditions boil down to

$$A_a B_a \leq 0 \text{ or } A_a C_a \leq 0. \quad (145)$$

We thus obtain

Lemma 3. Assume that (139) holds. Then (130) has no positive real zero if and only if

$$A_a B_a > 0 \text{ and } A_a C_a > 0, \quad (146)$$

and (134) has no positive real zero if and only if

$$A_b B_b > 0 \text{ and } A_b C_b > 0. \quad (147)$$

\square

We further examine the terms in (146). The condition $A_a B_a > 0$ expands to

$$\begin{cases} s^2 > \frac{(a-\mu)^2(b-\mu)}{a+2b-3\mu} & \text{if } \mu < \frac{a+b}{3} \text{ or } \mu > b \\ \text{false,} & \text{otherwise.} \end{cases} \quad (148)$$

The condition $A_a C_a > 0$ expands to

$$\begin{cases} s^2 > \frac{(a-\mu)^2(b-a)}{a+b-2\mu}, & \text{if } \mu < \frac{a+b}{2} \\ \text{false,} & \text{if } \frac{a+b}{2} \leq \mu \leq b \\ \text{true,} & \text{if } \mu > b. \end{cases} \quad (149)$$

We also note that the expressions $\frac{(a-\mu)^2(b-\mu)}{a+2b-3\mu}$ and $\frac{(a-\mu)^2(b-a)}{a+b-2\mu}$ as functions of μ intersect at the three points $\mu = a$ and

$$\mu = a \pm \frac{b-a}{\sqrt{2}} \quad (150)$$

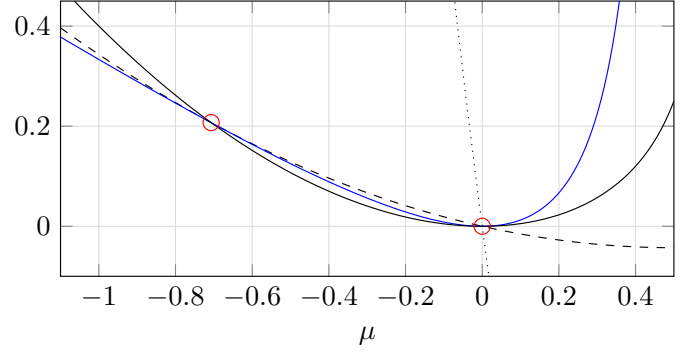


Fig. 18. The functions in Table II for $a = 0$ and $b = 1$.

cf. Table II. From (148)–(150), we can conclude that (146) is equivalent to

$$\begin{cases} s^2 > \frac{(a-\mu)^2(b-\mu)}{a+2b-3\mu} & \text{if } \mu < a - \frac{|a-b|}{\sqrt{2}} \\ s^2 > \frac{(a-\mu)^2(b-a)}{a+b-2\mu} & \text{if } a - \frac{|a-b|}{\sqrt{2}} \leq \mu < \frac{a+b}{2} \\ \text{false,} & \text{if } \frac{a+b}{2} \leq \mu \leq b \\ s^2 > \frac{(a-\mu)^2(b-\mu)}{a+2b-3\mu} & \text{if } \mu > b. \end{cases} \quad (151)$$

Likewise, we examine the terms in (147). (Because of the assumption $b > a$, we cannot simply exchange a and b in (151).) The condition $A_b B_b > 0$ expands to

$$\begin{cases} s^2 > \frac{(b-\mu)^2(a-\mu)}{b+2a-3\mu} & \text{if } \mu < a \text{ or } \mu > \frac{b+2a}{3} \\ \text{false,} & \text{otherwise.} \end{cases} \quad (152)$$

The condition $A_b C_b > 0$ expands to

$$\begin{cases} \text{true,} & \text{if } \mu < a \\ \text{false,} & \text{if } a \leq \mu \leq \frac{a+b}{2} \\ s^2 > \frac{(b-\mu)^2(a-b)}{a+b-2\mu} & \text{if } \mu > \frac{a+b}{2}. \end{cases} \quad (153)$$

The functions $\frac{(b-\mu)^2(a-\mu)}{b+2a-3\mu}$ and $\frac{(b-\mu)^2(a-b)}{a+b-2\mu}$ intersect at the points $\mu = b$ and

$$\mu = b \pm \frac{a-b}{\sqrt{2}}. \quad (154)$$

We conclude that (147) is equivalent to

$$\begin{cases} s^2 > \frac{(b-\mu)^2(a-\mu)}{b+2a-3\mu} & \text{if } \mu < a. \\ \text{false,} & \text{if } a \leq \mu \leq \frac{a+b}{2} \\ s^2 > \frac{(b-\mu)^2(a-b)}{a+b-2\mu} & \text{if } \frac{a+b}{2} < \mu \leq b + \frac{|a-b|}{\sqrt{2}} \\ s^2 > \frac{(b-\mu)^2(a-\mu)}{b+2a-3\mu} & \text{if } \mu > b + \frac{|a-b|}{\sqrt{2}}. \end{cases} \quad (155)$$

We have thus expanded Lemma 3 into

Lemma 4. Assume that (139) holds. Then (130) has no positive real zero if and only if (151) holds, and (134) has no positive real zero if and only if (155) holds. \square

For $\mu < \frac{a+b}{2}$, (155) is stricter than (151), and for $\mu > \frac{a+b}{2}$, (151) is stricter than (155). This allows us to combine (151) and (155) into

TABLE II
ORDERING OF CRITICAL FUNCTIONS IN THE PROOF OF THEOREM 2, CF. FIG. 18.

range	order
$\mu < a - \frac{b-a}{\sqrt{2}}$	$\frac{(a-\mu)^2(b-a)}{a+b-2\mu} < (3-\sqrt{8})(a-\mu)(b-\mu) < \frac{(a-\mu)^2(b-\mu)}{a+2b-3\mu} < (3+\sqrt{8})(a-\mu)(b-\mu)$
$a - \frac{b-a}{\sqrt{2}} < \mu < a$	$\frac{(a-\mu)^2(b-\mu)}{a+2b-3\mu} < \frac{(a-\mu)^2(b-a)}{a+b-2\mu} < (3-\sqrt{8})(a-\mu)(b-\mu) < (3+\sqrt{8})(a-\mu)(b-\mu)$
$a < \mu < \frac{a+b}{2}$	$(3+\sqrt{8})(a-\mu)(b-\mu) < (3-\sqrt{8})(a-\mu)(b-\mu) < \frac{(a-\mu)^2(b-\mu)}{a+2b-3\mu} < \frac{(a-\mu)^2(b-a)}{a+b-2\mu}$

Lemma 5. Assume that (139) holds. Then at least one of (130) and (134) has no positive real zeros if and only if

$$\begin{cases} s^2 > \frac{(a-\mu)^2(b-\mu)}{a+2b-3\mu} & \text{if } \mu < a - \frac{|a-b|}{\sqrt{2}} \\ s^2 > \frac{(a-\mu)^2(b-a)}{a+b-2\mu} & \text{if } a - \frac{|a-b|}{\sqrt{2}} \leq \mu < \frac{a+b}{2} \\ s^2 > \frac{(b-\mu)^2(a-b)}{a+b-2\mu} & \text{if } \frac{a+b}{2} < \mu \leq b + \frac{|a-b|}{\sqrt{2}} \\ s^2 > \frac{(b-\mu)^2(a-\mu)}{b+2a-3\mu} & \text{if } \mu > b + \frac{|a-b|}{\sqrt{2}}. \end{cases} \quad (156)$$

Using Table II, Lemma 5 and Lemma 2 can be combined into

Lemma 6. At least one of (130) and (134) has no positive real zeros if and only if

$$\begin{cases} s^2 > (3-\sqrt{8})(a-\mu)(b-\mu) & \text{if } \mu < a - \frac{|a-b|}{\sqrt{2}} \\ s^2 > \frac{(a-\mu)^2(b-a)}{a+b-2\mu} & \text{if } a - \frac{|a-b|}{\sqrt{2}} \leq \mu < \frac{a+b}{2} \\ s^2 > \frac{(b-\mu)^2(a-b)}{a+b-2\mu} & \text{if } \frac{a+b}{2} < \mu \leq b + \frac{|a-b|}{\sqrt{2}} \\ s^2 > (3-\sqrt{8})(a-\mu)(b-\mu) & \text{if } \mu > b + \frac{|a-b|}{\sqrt{2}}. \end{cases} \quad (157)$$

Finally, we note from Table II that, for $\mu < (a+b)/2$, (120) is implied by (157). Likewise, for $\mu > (a+b)/2$, (122) is also implied by (157), which completes the proof.

ACKNOWLEDGMENT

The authors would like to thank Gian Marti and Hampus Malmberg for valuable discussions.

REFERENCES

- [1] A. H. Land and A. G. Doig, "An automatic method of solving discrete programming problems," *Econometrica*, vol. 28, no. 3, pp. 497–520, 1960.
- [2] L. A. Wolsey and G. L. Nemhauser, *Integer and Combinatorial Optimization*. John Wiley & Sons, 1999.
- [3] R. P. Aguilera and D. E. Quevedo, "On stability and performance of finite control set MPC for power converters," in *IEEE Workshop on Predictive Control of Electrical Drives and Power Electronics*, 2011, pp. 55–62.
- [4] T. Geyer and D. E. Quevedo, "Multistep finite control set model predictive control for power electronics," *IEEE Trans. Power Electron.*, vol. 29, no. 12, pp. 6836–6846, 2014.
- [5] T. Dorfling, H. du Toit Mouton, T. Geyer, and P. Karamanakos, "Long-horizon finite-control-set model predictive control with nonrecursive sphere decoding on an FPGA," *IEEE Trans. Power Electron.*, vol. 35, no. 7, pp. 7520–7531, 2020.
- [6] S. Sparrer and R. F. H. Fischer, "Adapting compressed sensing algorithms to discrete sparse signals," in *18th International ITG Workshop on Smart Antennas*, 2014, pp. 1–8.
- [7] T. Ikeda, M. Nagahara, and S. Ono, "Discrete-valued control of linear time-invariant systems by sum-of-absolute-values optimization," *IEEE Trans. Autom. Control*, vol. 62, no. 6, pp. 2750–2763, 2016.
- [8] S. Russel and P. Norvig, *Artificial intelligence: A modern approach*. Pearson Education Limited, 2013.
- [9] M. Pincus, "Letter to the editor – a Monte Carlo method for the approximate solution of certain types of constrained optimization problems," *Operations Research*, vol. 18, no. 6, pp. 1225–1228, 1970.
- [10] M. E. Tipping, "Sparse Bayesian learning and the relevance vector machine," *Journal of Machine Learning Research*, vol. 1, pp. 211–244, 2001.
- [11] M. E. Tipping and A. C. Faul, "Fast marginal likelihood maximisation for sparse Bayesian models," in *Proc. of the Ninth International Workshop on Artificial Intelligence and Statistics*, 2003, pp. 3–6.
- [12] D. P. Wipf and B. D. Rao, "Sparse Bayesian learning for basis selection," *IEEE Trans. Signal Process.*, vol. 52, no. 8, pp. 2153–2164, 2004.
- [13] D. P. Wipf and S. S. Nagarajan, "A new view of automatic relevance determination," in *Advances in Neural Information Processing Systems*, 2008, pp. 1625–1632.
- [14] H.-A. Loeliger, B. Ma, H. Malmberg, and F. Wadehn, "Factor graphs with NUV priors and iteratively reweighted descent for sparse least squares and more," in *Proc. Int. Symp. Turbo Codes & Iterative Inform. Process. (ISTC)*, 2018, pp. 1–5.
- [15] F. Bach, R. Jenatton, J. Mairal, and G. Obozinski, "Optimization with sparsity-inducing penalties," *Foundations and Trends in Machine Learning*, vol. 4, no. 1, pp. 1–106, 2012.
- [16] J. Dai, A. Liu, and H. C. So, "Sparse Bayesian learning approach for discrete signal reconstruction," 2019, unpublished, arXiv:1906.00309.
- [17] H.-A. Loeliger, L. Bruderer, H. Malmberg, F. Wadehn, and N. Zalmai, "On sparsity by NUV-EM, Gaussian message passing, and Kalman smoothing," in *Information Theory and Applications Workshop (ITA)*, La Jolla, CA, 2016, pp. 1–10.
- [18] H.-A. Loeliger, "An introduction to factor graphs," *IEEE Signal Process. Mag.*, vol. 21, no. 1, pp. 28–41, 2004.
- [19] P. Stoica and Y. Selén, "Cyclic minimizers, majorization techniques, and the expectation-maximization algorithm: a refresher," *IEEE Signal Process. Mag.*, vol. 21, no. 1, pp. 112–114, 2004.
- [20] G. J. Bierman, *Factorization Methods for Discrete Sequential Estimation*. Academic Press, 1977, vol. 128.
- [21] R. Giri and B. Rao, "Type I and type II Bayesian methods for sparse signal recovery using scale mixtures," *IEEE Trans. Signal Process.*, vol. 64, no. 13, pp. 3418–3428, 2016.
- [22] B. E. Boser and B. A. Wooley, "The design of sigma-delta modulation analog-to-digital converters," *IEEE J. Solid-State Circuits*, vol. 23, no. 6, pp. 1298–1308, 1988.
- [23] Flappy Bird. Accessed 09-October-2020. [Online]. Available: https://en.wikipedia.org/wiki/Flappy_Bird
- [24] T. P. Minka, "Expectation propagation for approximate Bayesian inference," *Proc. 17th Annual Conf. on Uncertainty in Artificial Intelligence (UAI-01)*, vol. 17, pp. 362–369, 2001.
- [25] J. Hu, H.-A. Loeliger, J. Dauwels, and F. Kschischang, "A general computation rule for lossy summaries/messages with examples from equalization," *Proc. 44th Allerton Conf. on Communication, Control, and Computing*, 2006.
- [26] M. Frey and H.-A. Loeliger, "On the static resolution of digitally-corrected analog-to-digital and digital-to-analog converters with low-precision components," *IEEE Trans. Circuits & Systems I*, vol. 54, no. 1, pp. 229–237, 2007.